photonics

MDPI

Communication

Intra-Cavity Cascaded Pumped 946/1030 nm Dual-Wavelength Vortex Laser Using a Spot-Defect Mirror

Yashuai Yang, Yongliang Li *, Xinyi Zhu, Chi Wang and Chao Yang

School of Opto-Electronics Engineering, Changchun University of Science and Technology, Changchun 130022, China; yangyashuai@mails.cust.edu.cn (Y.Y.); zhuxinyi@mails.cust.edu.cn (X.Z.); wangchi@mails.cust.edu.cn (C.W.); yangchao@cust.edu.cn (C.Y.)

* Correspondence: liyongliang@cust.edu.cn

Abstract: Due to their unique properties, vortex lasers have high application value in frontier fields such as optical micromanipulation, super-resolution imaging, quantum entanglement, and optical communication. In this study, we demonstrated a 946/1030 nm Laguerre-Gaussian (LG_{01}) mode dual-wavelength vortex laser by using an intracavity cascade pumped structure and a spot-defect output mirror. Using a coaxial linear cavity structure, the 808 nm laser diode (LD) was used to end-pump the Nd:YAG crystal to generate a 946 nm laser and then use it to directly pump the Yb:YAG crystal in the cavity to generate a 1030 nm laser, and finally a 946/1030 nm dual-wavelength laser came out. By making a spot defect in the center of the output mirror to suppress the oscillation of the fundamental Gaussian mode laser and carefully adjusting the position of the laser crystals, the LG_{01} mode dual-wavelength vortex laser was output in single handedness. When the pump power was 40 W, the total output was 664 mW (356 and 308 mW at 946 and 1030 nm LG_{01} mode vortex lasers), and the total optical-optical conversion efficiency was 1.7%; the output power fluctuations of 946 and 1030 nm LG_{01} mode vortex lasers within 1 h were 3.43% and 3.13%, respectively; the beam quality factors M^2 of 946 and 1030 nm LG_{01} mode vortex lasers were 2.35 and 2.40, respectively. It was proved that the generated dual-wavelength vortex laser had the wavefront phase $\exp(i\phi)$ by the self-interference method.

Keywords: dual-wavelength; LG_{01} mode; spot-defect mirror; intra-cavity pumped

Citation: Yang, Y.; Li, Y.; Zhu, X.; Wang, C.; Yang, C. Intra-Cavity Cascaded Pumped 946/1030 nm Dual-Wavelength Vortex Laser Using a Spot-Defect Mirror. *Photonics* **2023**, *10*, 554. https://doi.org/10.3390/photonics10050554

Received: 5 April 2023
Revised: 26 April 2023
Accepted: 5 May 2023
Published: 10 May 2023

1. Introduction

Compared with fundamental Gaussian beams, LG beams have an annular-shaped profile, a spiral wavefront, and orbital angular momentum [1,2]. Due to their unique characteristics, LG beams have been applied in a series of frontier applications. In the early days, LG beams were applied to optical trapping and manipulation [3,4], stimulated emission depletion microscopy [5,6], quantum information [7,8], and space multiplexing optical communications [9,10]. Recently, with the continuous development of LG beam research, applications in several new fields have been found in terms of LG beams, such as the creation of micro- and nano-needle structures [11], generation of magnetic skyrmions [12], in-line nanoscale defect inspection with high sensitivity and robustness [13], reliable ptychographic imaging of highly periodic structures [14], etc. In addition, the concept of vortex light is introduced into the dual-wavelength laser, and the dual-wavelength LG-mode laser is brought into operation as a new type of laser to further improve the performance of existing applications or to bring forth innovative progress in applications. For example, dual-frequency 2-fold multiplexed vortex light is used as the detection beam to measure the angular velocity, successfully reducing the low frequency noise signal generated when using single-frequency vortex light measurements and allowing direct access to the direction of rotation [15]. Additionally, based on the advantage of high power density in the cavity [16], the dual-wavelength LG beam can be used for sum-frequency operation in the resonant cavity with high efficiency to further obtain the vortex beam in the blue wavelength band. Therefore, the study of dual-wavelength LG mode lasers is one of the important research directions for vortex optical lasers.

Currently, the methods of LG beam generation are mainly divided into extra-cavity passive methods and intra-cavity active methods. Hermie-Gaussian (HG) beams can be converted into LG beams through a cylindrical lens mode converter outside the resonant cavity [17], and fundamental Gaussian beams can be converted into LG beams through computer-generated holograms [18], spatial light modulators [19], spiral phase plates [20], optical wedges [21], metasurfaces [22], and other optical elements outside the resonant cavity. However, these passive generation methods of LG beams have certain disadvantages, such as high cost, low damage threshold, and generally poor quality of the beams obtained. In recent years, many active generation methods have been used to suppress the oscillation of fundamental Gaussian beams in the resonance of solid-state lasers to achieve the direct output of LG mode lasers, such as end-pumping gain medium by the annular beam [23–25], rotating gain medium induced off-axis pumping [26] and using a spot-defect cavity mirror [27–29]. At present, LG beams are generally obtained based on He-Ne Yb-, Nd-, and Er-doped gain medium, and the wavelengths of the LG beams obtained are very limited, mainly 632, 1030, 1064, and 1645 nm. The vast majority of the obtained LG beam wavelengths are output at a single laser wavelength. So far, only A. J. Lee et al. realized LG_{01} mode dual-wavelength output (1063 nm fundamental beam and 1173 nm Stokes beam) in a $Nd:GdVO_4$ self-Raman laser based on a defective spot on the output coupler [30]. Besides the one mentioned, there are no other reports on the research of active methods to generate LG_{01} mode dual-wavelength lasers.

In this paper, we used the intracavity cascade pumping structure, which contains two resonant cavities at 946 and 1030 nm. The two resonant cavities share a common output mirror, and the 1030 nm resonant cavity is located within the 946 nm resonant cavity. The 808 nm LD was used to end-pump the Nd:YAG crystal to generate a 946 nm laser, then use it to directly pump the Yb:YAG crystal in the cavity to generate a 1030 nm laser, and finally produce a 946/1030 nm dual-wavelength laser output coaxially. Compared to schemes based on a single gain medium and nonlinear frequency conversion to generate dual-wavelength lasers, intracavity cascade pumping schemes can effectively avoid the problems of gain competition between spectral lines and strict phase matching [31,32]. By creating a spot defect in the center of the output mirror to suppress the oscillation of the fundamental Gaussian mode laser, a 946/1030 nm LG_{01} mode dual-wavelength vortex laser was successfully achieved. After experimental optimization, the output power of the 946 and 1030 nm LG_{01} mode vortex lasers were 356 and 308 mW, respectively, when the pump power was 40 W and the dual-wavelength vortex laser was output in single handedness.

2. Experiment Setup

The experimental setup of a 946/1030 nm LG_{01} mode dual-wavelength vortex laser using a spot-defect mirror is demonstrated in Figure 1. The pump source is an 808 nm fiber-coupled (0.22 NA, 200 µm core diameter) LD. The pump laser is converged to the front surface of the Nd:YAG crystal using a coupling lens set, which consists of two lenses with the same focal length. The Nd:YAG crystal (the diameter and length are 4 and 3 mm, respectively, and the doping concentration is 1%) is coated with 808 nm and 946 nm antireflection films on the front surface and a 946 nm antireflection film on the back surface. The Yb:YAG crystals (the diameter and length are 4 and 2 mm, respectively, and the doping concentration is 0.5%) are coated with 946 nm and 1030 nm antireflection films on both the front and back surfaces. Although the absorption coefficient of the Yb:YAG crystal is low for the 946 nm laser, the high intracavity pump power ensures the oscillation of the 1030 nm laser. In addition, the lower doping concentration helps to reduce thermal effects and losses from reabsorption in the quasi-three-level system. Both laser crystals are wrapped with indium foil and installed in a water-cooled fixture made of purple copper, where the temperature is controlled at 15 °C. The 946 nm resonant cavity consists of a total reflective mirror M_1 and a common output mirror M_2, with a cavity length of 80 mm. The 1030 nm sub-resonant cavity consists of a total reflective mirror M_3 and a common output mirror M_2, with a cavity length of 40 mm. M_1 and M_3 are both flat-concave mirrors with a radius of curvature of 300 mm, and M_2 is a flat-flat mirror. The M_1 is coated with 808 and 1064 nm antireflection films on the front and back surfaces, and a 946 nm high-reflection film on the back surface. The 1064 nm antireflection film effectively suppresses the energy level transition ($^4F_{3/2} \rightarrow {}^4I_{11/2}$) at the 1064 nm laser. The M_3 is coated with 946 nm antireflection film on the front surface and 946 nm antireflection film and 1030 nm high-reflection film on the back surface. The 355 nm ultraviolet laser is used to etch off the coating layers at the center of the circle on the surface of the M_2, forming a spot defect with a diameter of about 170 µm. Since the spot defect can produce large losses in the output laser, an output mirror with low transmission rates is used. The transmittance of M_2 to 946 and 1030 nm is 1.9% and 2.8%, respectively. The remaining 808 nm pump laser in the output laser is absorbed by the RGB830 glass filter. The azimuthal symmetry inside the cavity is broken by micro-adjusting the angles of Nd:YAG and Yb:YAG crystals [29,33], so that the vortex laser of different handedness has differential losses to obtain the dual-wavelength vortex laser with single handedness. The output laser is divided into 946 and 1030 nm LG_{01} mode vortex lasers by dichroic mirror M_4.

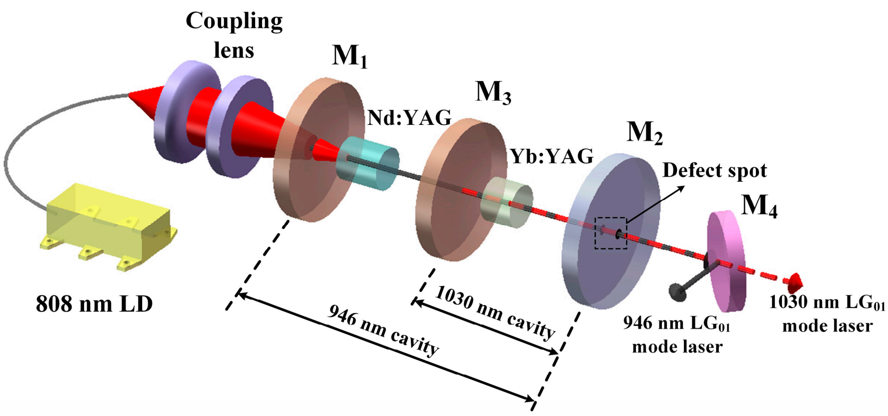

Figure 1. The experimental setup of a 946/1030 nm LG_{01} mode dual-wavelength vortex laser using a spot-defect mirror.

3. Experimental Results and Discussion

By moving the lateral position of the output mirror M_2 so that the center of the spot defect moves to the optical axis of the resonant cavity and then adjusting the front and rear positions of the focusing mirror in the coupling lens set to regulate the pump laser in the Nd:YAG crystal to match the LG_{01} mode vortex laser, an annular-shaped beam was obtained in the whole pump range. The vortex laser of opposite handedness has the same threshold pumping power in the resonant cavity with better symmetric characteristics, so theoretically, the vortex laser of both handedness can be output from the resonant cavity at the same time. In order to reduce the insertion loss caused by additional components, the position of the laser crystals was micro-adjusted to make the dual-wavelength laser output single handed. The obtained 946 and 1030 nm LG vortex lasers were converted to HG lasers by a mode converter consisting of two cylindrical lenses of the same focal length f (spacing of $\sqrt{2}f$), where the 946 nm LG vortex laser is adjusted to a direction parallel to the optical axis by a reflector to facilitate the measurement. In addition, the 946 nm LG vortex laser is reflected by the dichroic mirror M_4 and re-reflected by the reflector, and its handedness is adjusted back to the original handedness of the output from the M_2. The number of nodal lines in the HG beam and the topological charge of the vortex laser are equal. The change in direction of the long axis of the HG laser is used to determine whether the handedness of the vortex laser has changed. The number of node lines in the HG beams at 946 and 1030 nm by the mode converter is 1, and the long-axis direction remains constant throughout the pumping range. The results turn out that the number of topological charges for the dual-wavelength vortex laser were both 1, and the dual-wavelength vortex laser was output in single handedness. The obtained spots of the 946 nm and 1030 nm LG_{01} mode vortex lasers and the spots of the HG_{01} mode laser at different pumping power states are shown in Figure 2.

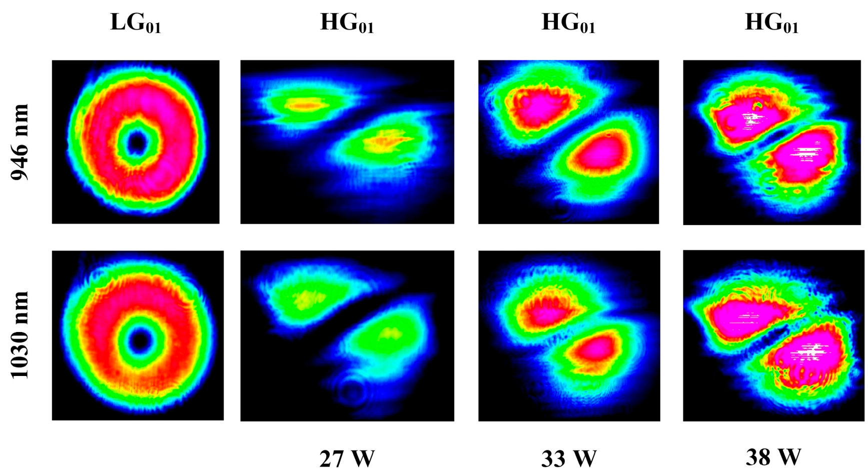

Figure 2. The spots of the 946 nm and 1030 nm LG_{01} mode vortex lasers and the spots of the HG_{01} mode laser at different pumping power states.

The wavefront phases of the 946 and 1030 nm LG_{01} mode vortex lasers were measured by a self-interferometric method based on a Michelson interferometer, and the optical path diagram of the measurement setup is shown in Figure 3a [29]. The vortex beam is first divided into a reflected beam and a transmitted beam through the beam splitter G_1, where the reflected beam is reflected by M_1 and then passed through the beam splitter G_1 again; the transmitted beam is passed through the compensation plate G_2, reflected by the reflector M_2, passed through the compensation plate G_2 again, and then reflected by the beam splitter G_1, and finally the two beams enter the CCD in a non-co-linear way to interfere. By adjusting the front and rear positions of the reflector M_1 to make the optical paths of the two channels equal. Using this device, the measured self-interference patterns of the 946 and 1030 nm LG_{01} mode vortex lasers are shown in Figure 3b,c, respectively. The measured interferograms both contain a pair of opposite Y-shaped stripes, indicating that the generated dual-wavelength lasers both contain the phase of the wave front $\exp(i\phi)$.

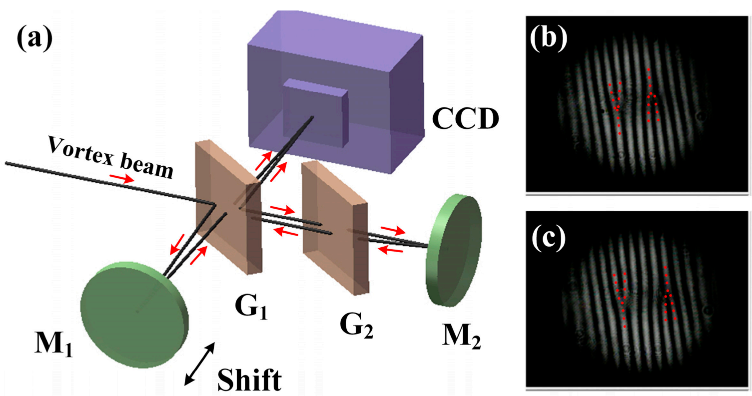

Figure 3. (**a**) The schematic diagram of the optical path of the wavefront phase detection device; the self-interference pattern of the (**b**) 946 nm and (**c**) 1030 nm LG_{01} vortex lasers. (Note: Use red dots to mark the Y-shaped stripes).

The spectrum of the output laser was measured using a fiber-optic spectrometer (StellarNet, BW-UVN-50), and the result is shown in Figure 4. As can be seen from the figure, the central wavelengths of the dual-wavelength laser are 946.48 and 1029.56 nm, respectively.

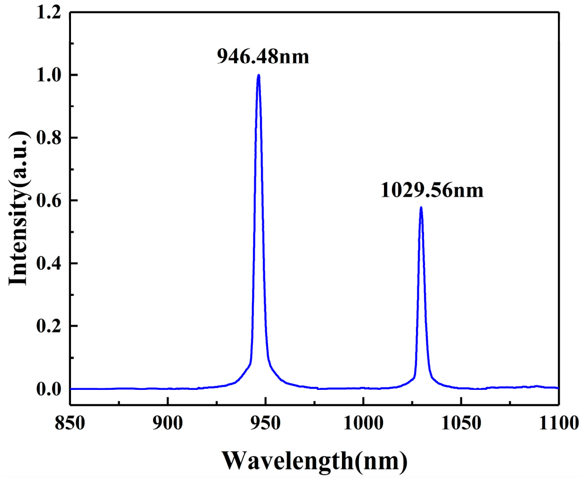

Figure 4. The spectrogram of a dual-wavelength vortex laser.

The relationship between the output power of the 946 and 1030 nm LG_{01} mode vortex lasers and the incident pump power was further tested, and the results are shown in Figure 5. When the pump power is 20.2 W, the 946 nm LG_{01} mode laser starts to output, and when the pump light power is increased to 25.6 W, the 946 and 1030 nm LG_{01} mode vortex lasers start to output simultaneously. The maximum output power of the 946 and 1030 nm LG_{01} mode vortex lasers is 356 and 308 mW, respectively, when the pump power is 40 W. The total optical-optical conversion efficiency is 1.7%. Additionally, based on the intracavity cascade pumping scheme, a combination of Nd:$GdVO_4$ and Nd:YVO_4 crystals was used to generate 912 and 1064 nm TEM_{00} mode dual-wavelength lasers with threshold pump powers of 15 and 17 W, respectively [34]. In contrast, the main reason for the high threshold power of the dual-wavelength vortex laser in this paper can be attributed to the fact that the output mirror with a point defect imposes some loss on the dual-wavelength vortex laser operation.

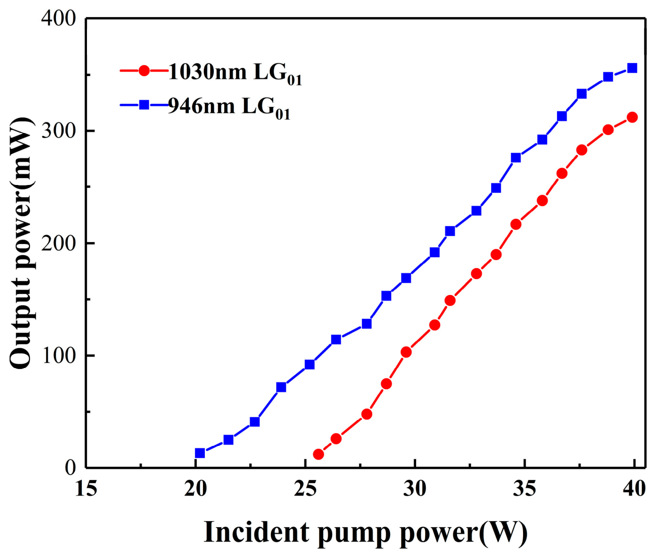

Figure 5. The relationship between the output power of the 946/1030 nm LG_{01} mode vortex laser and the incident pump power.

The power fluctuation of the dual-wavelength vortex laser was tested when the laser output power was at its maximum, and the test results are shown in Figure 6a. The output power of the 946 and 1030 nm LG_{01} mode vortex lasers was recorded simultaneously every 2 min for a total test time of 1 h. The power fluctuations of the 946 and 1030 nm LG_{01} mode vortex lasers were 3.43% and 3.13%, respectively. The fluctuation of the total output power was 0.84%, which is smaller than the fluctuation of the 946 and 1030 nm LG_{01} mode vortex lasers, respectively. In addition, we found the power fluctuation of the 808 nm pump laser with time, which fluctuated by 0.37%, and the test result is shown in Figure 6b. When the power of one wavelength of vortex laser increases, the power of the other wavelength of vortex laser decreases, which makes the total output power fluctuate very little. This phenomenon indicates that there is a weak competition between the output power of dual-wavelength vortex lasers based on the intracavity cascade pumping structure.

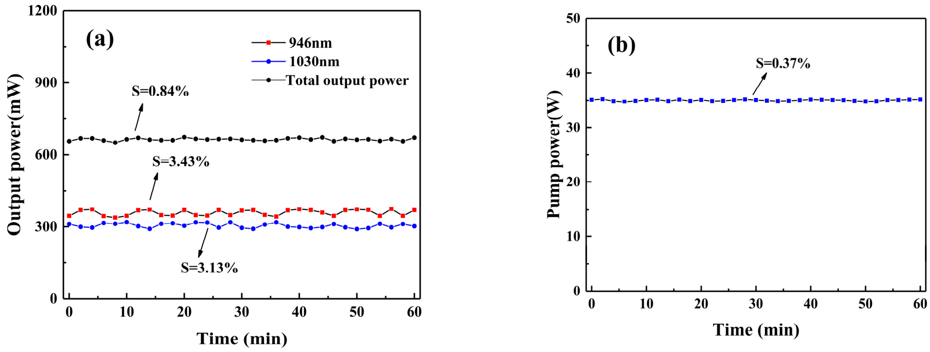

Figure 6. The power fluctuation of (**a**) 946/1030 nm LG_{01} mode dual-wavelength vortex laser and (**b**) pump laser with time.

In addition, the variation of the beam quality factor of a dual-wavelength vortex laser with pump power was measured, and the test result is shown in Figure 7a. The beam quality factor M^2 of the 946 nm and 1030 nm LG_{01} mode vortex light increased from 2.19 to 2.35 and 2.20 to 2.40 with increasing pump power, respectively. Due to the increase in pump power, the increase in thermal effect is one of the main reasons for the increase in beam quality factor M^2 of dual-wavelength vortex laser. The test result of the beam quality factor M^2 of the dual-wavelength vortex laser at the maximum output power is shown in Figure 7b. The beam quality factors M^2 of the 946 and 1030 nm LG_{01} mode vortex lasers were 2.35 and 2.40, respectively, and the theoretical value of the beam quality factor M^2 of the LG_{01} mode vortex laser is 2.

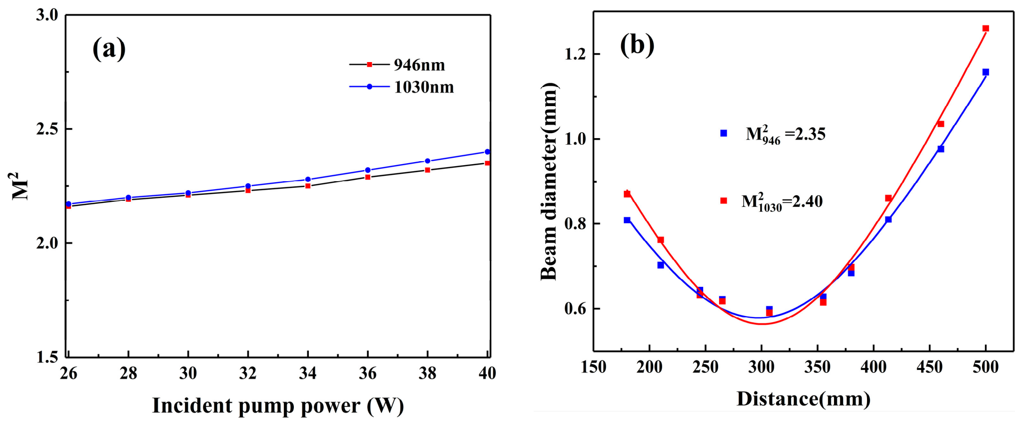

Figure 7. (**a**) The variation of beam quality factor M^2 of a 946/1030 nm LG_{01} mode dual-wavelength vortex laser with pump power; (**b**) beam quality factor test results at maximum output power.

4. Conclusions

In this study, a 946/1030 nm LG_{01} mode dual-wavelength vortex laser was demonstrated. Based on the intracavity cascade pumping structure, the 808 nm LD was used to end-pump the Nd:YAG crystal to generate the 946 nm laser, and then it was used to directly pump the Yb:YAG crystal in the cavity to generate the 1030 nm laser, and finally the 946/1030 nm dual-wavelength laser was obtained. This structure avoids competition between the two output spectral lines. The precision etching technique was applied to create a spot defect in the center of the output mirror, which suppresses the oscillation of the fundamental Gaussian mode laser and ensures the oscillation of the LG_{01} mode vortex laser. In addition, the position of the laser crystals was fine-adjusted to produce a sufficient loss difference between the vortex lasers with opposite handedness so that a dual-wavelength vortex laser was output in single handedness. When the pump power was 40 W, the output power of the 946 and 1030 nm LG_{01} mode vortex lasers was 356 and 308 mW, respectively, and the total optical-optical conversion efficiency was 1.7%. The power fluctuations of the 946 and 1030 nm LG_{01} mode vortex lasers at the maximum output power were 3.43% and 3.13% in 1 h, respectively, and the fluctuation of the total output power was 0.84%. The fluctuation of the total output power is smaller than that of the 946 and 1030 nm LG_{01} mode vortex lasers, indicating that there is some competition between the output power of the dual-wavelength vortex lasers. The beam quality factors M^2 were 2.35 and 2.40 for the 946 and 1030 nm LG_{01} mode vortex lasers at maximum output power, respectively. Both the 946 and 1030 nm interferograms measured by the self-interference method contain a pair of opposite Y-shaped stripes, indicating that the generated dual-wavelength lasers both contain the wavefront phase $\exp(i\phi)$. Compared with the fundamental Gaussian laser, the vortex laser can significantly reduce the beam diffusion caused by atmospheric turbulence. Therefore, by replacing the conventional fundamental Gaussian mode dual-wavelength laser, the dual-wavelength vortex laser will significantly improve performance in remote sensing, topography, and other fields. In addition, the dual-wavelength vortex laser developed in this paper can be used for further intracavity sum-frequency experiments to obtain the vortex laser in the blue wavelength band. As vortex lasers are put into use in an increasingly wide range of applications, it is important to improve the wavelength versatility of vortex laser sources.

Author Contributions: Conceptualization, Y.Y. and Y.L.; Data curation, Y.Y.; Formal analysis, Y.Y.; Funding acquisition, Y.L. and C.Y.; Investigation, Y.Y. and X.Z.; Methodology, Y.Y.; Project administration, Y.L. and C.Y.; Resources, Y.L.; Software, Y.Y. and X.Z.; Supervision, Y.Y. and Y.L.; Validation, Y.Y., Y.L. and C.W.; Visualization, Y.Y.; Writing—original draft, Y.Y.; Writing—review and editing, Y.Y., X.Z. and Y.L. All authors have read and agreed to the published version of the manuscript.

Funding: This research was funded by the Natural Science Foundation of China (Grant No. 62075018), Jilin Provincial Natural Science Foundation (No. 20220101359JC), the 111 Project of China (D17017), and the National Demonstration Center for Experimental Opto-Electronic Engineering Education.

Institutional Review Board Statement: Not applicable.

Informed Consent Statement: Not applicable.

Data Availability Statement: Not applicable.

Conflicts of Interest: The authors declare no conflict of interest.

References

1. Allen, L.; Beijersbergen, M.W.; Spreeuw, R.J.C.; Woerdman, J.P. Orbital angular momentum of light and the transformation of Laguerre-Gaussian laser modes. *Phys. Rev. A* **1992**, *45*, 8185–8189. [CrossRef] [PubMed]
2. Harris, M.; Hill, C.A.; Tapster, P.R.; Vaughan, J.M. Laser modes with helical wave fronts. *Phys. Rev. A* **1994**, *49*, 3119–3122. [CrossRef] [PubMed]
3. Čižmár, T.; Brzobohatý, O.; Dholakia, K.; Zemánek, P. The holographic optical micro-manipulation system based on counter-propagating beams. *Laser Phys. Lett.* **2011**, *8*, 50–56. [CrossRef]
4. Padgett, M.; Bowman, R. Tweezers with a twist. *Nat. Photonics* **2011**, *5*, 343–348. [CrossRef]
5. Vicidomini, G.; Bianchini, P.; Diaspro, A. STED super-resolved microscopy. *Nat. Methods* **2018**, *15*, 173–182. [CrossRef] [PubMed]
6. Hell, S.W.; Wichmann, J. Breaking the diffraction resolution limit by stimulated emission: Stimulated-emission-depletion fluorescence microscopy. *Opt. Lett.* **1994**, *19*, 780–782. [CrossRef] [PubMed]
7. Franke-Arnold, S.; Allen, L.; Padgett, M. Advances in optical angular momentum. *Laser Photonics Rev.* **2008**, *2*, 299–313. [CrossRef]
8. Perez-Garcia, B.; Francis, J.; McLaren, M.; Hernandez-Aranda, R.I.; Forbes, A.; Konrad, T. Quantum computation with classical light: The Deutsch Algorithm. *Phys. Lett. A* **2015**, *379*, 1675–1680. [CrossRef]

9. Willner, A.E.; Huang, H.; Yan, Y.; Ren, Y.; Ahmed, N.; Xie, G.; Bao, C.; Li, L.; Cao, Y.; Zhao, Z.; et al. Optical communications using orbital angular momentum beams. *Adv. Opt. Photon.* **2015**, *7*, 66–106. [CrossRef]
10. Huang, H.; Xie, G.D.; Yan, Y.; Ahmed, N.; Ren, Y.X.; Yue, Y.; Rogawski, D.; Willner, M.J.; Erkmen, B.I.; Birnbaum, K.M.; et al. 100 Tbit/s free-space data link enabled by three-dimensional multiplexing of orbital angular momentum, polarization, and wavelength. *Opt. Lett.* **2014**, *39*, 197–200. [CrossRef]
11. Syubaev, S.; Zhizhchenko, A.; Kuchmizhak, A.; Porfirev, A.; Pustovalov, E.; Vitrik, O.; Kulchin, Y.; Khonina, S.; Kudryashov, S. Direct laser printing of chiral plasmonic nanojets by vortex beams. *Opt. Express* **2017**, *25*, 10214–10223. [CrossRef]
12. Polyakov, O.P.; Gonoskov, I.A.; Stepanyuk, V.S.; Gross, E.K.U. Generation of magnetic skyrmions by focused vortex laser pulses. *J. Appl. Phys.* **2020**, *127*, 073904. [CrossRef]
13. Wang, B.; Tanksalvala, M.; Zhang, Z.; Esashi, Y.; Jenkins, N.W.; Murnane, M.M.; Kaptern, H.C.; Liao, C.-T. Coherent Fourier scatterometry using orbital angular momentum beams for defect detection. *Opt. Express* **2020**, *29*, 3342–3358. [CrossRef] [PubMed]
14. Wang, B.; Brooks, N.J.; Johnsen, P.C.; Jenkins, N.W.; Esashi, Y.; Binnie, I.; Tanksalvala, M.; Kapteyn, H.C.; Murnane, M.M. High-fidelity ptychographic imaging of highly periodic structures enabled by vortex high harmonic beams. *arXiv* **2023**, arXiv:2301.05563.
15. Li, Z.; Liu, T.; Ren, Y.; Qiu, S.; Wang, C.; Wang, H. Direction-sensitive detection of spinning object using dual-frequency vortex light. *Opt. Express* **2021**, *29*, 7453–7463. [CrossRef] [PubMed]
16. Hu, C.W.; Li, Y.L.; Hu, W.W.; Chen, Z.W.; Sun, X.T. Intracavity cascade pumped 493.1nm blue laser. *Optik* **2020**, *219*, 165126. [CrossRef]
17. Courtial, J.; Padgett, M.J. Performance of a cylindrical lens mode converter for producing Laguerre–Gaussian laser modes. *Opt. Commun.* **1999**, *159*, 13–18. [CrossRef]
18. Heckenberg, N.R.; McDuff, R.; Smith, C.P.; White, A.G. Generation of optical phase singularities by computer-generated holograms. *Opt. Lett.* **1992**, *17*, 221–223. [CrossRef]
19. Matsumoto, N.; Ando, T.; Inoue, T.; Ohtake, Y.; Fukuchi, N.; Hara, T. Generation of high-quality higher-order Laguerre-Gaussian beams using liquid-crystal-on-silicon spatial light modulators. *J. Opt. Soc. Am. A* **2008**, *25*, 1642–1651. [CrossRef]
20. Xin, J.; Dai, K.; Zhong, L.; Na, Q.; Gao, C. Generation of optical vortices by using spiral phase plates made of polarization dependent devices. *Opt. Lett.* **2014**, *39*, 1984–1987. [CrossRef]
21. Shvedov, V.G.; Izdebskaya, Y.V.; Alekseev, A.N.; Volyar, A.V. The formation of optical vortices in the course of light diffraction on a dielectric wedge. *Tech. Phys. Lett.* **2002**, *28*, 256–259. [CrossRef]
22. Yang, Y.M.; Wang, W.Y.; Moitra, P.; Kravchenko, I.I.; Briggs, D.P.; Valentine, J. Dielectric Meta-Reflectarray for Broadband Linear Polarization Conversion and Optical Vortex Generation. *Nano Lett.* **2014**, *14*, 1394–1399. [CrossRef] [PubMed]
23. Zhao, Y.G.; Liu, Q.Y.; Zhou, W.; Shen, D.Y. ~1 mJ pulsed vortex laser at 1645 nm with well-defined helicity. *Opt. Express* **2016**, *24*, 15596–15602. [CrossRef]
24. Li, G.Y.; Xia, K.G.; Wang, Z.Y.; Shen, H.; Shirakawa, A.; Ueda, K.-I.; Li, J.L. Conical refraction, for annular pumping of an efficient vortex Nd:YAG laser. *Laser Phys. Lett.* **2017**, *14*, 075001. [CrossRef]
25. He, H.S.; Chen, Z.; Li, H.B.; Dong, J. Low-threshold, nanosecond, high-repetition-rate vortex pulses with controllable helicity generated in Cr,Nd:YAG self-Q-switched microchip laser. *Laser Phys.* **2018**, *28*, 055802. [CrossRef]
26. Huang, X.X.; Xu, B.; Cui, S.W.; Xu, H.Y.; Cai, Z.P.; Chen, L.X. Direct Generation of Vortex Laser by Rotating Induced Off-Axis Pumping. *IEEE J. Sel. Top. Quantum Electron.* **2018**, *24*, 1601606. [CrossRef]
27. Uesugi, Y.; Sato, S.; Kozawa, Y. Direct generation of the lowest-order vortex beam using a spot defect mirror in the ultraviolet region. *Opt. Lett.* **2020**, *45*, 2115–2118. [CrossRef]
28. Kano, K.; Kozawa, Y.; Sato, S. Generation of a Purely Single Transverse Mode Vortex Beam from a He-Ne Laser Cavity with a Spot-Defect Mirror. *Int. J. Opt.* **2011**, *2012*, 359141. [CrossRef]
29. Qiao, Z.; Xie, G.Q.; Wu, Y.H.; Yuan, P.; Ma, J.G.; Qiao, L.J.; Fan, D.Y. Generating High-Charge Optical Vortices Directly from Laser Up to 288th Order. *Laser Photon. Rev.* **2018**, *12*, 1800019. [CrossRef]
30. Lee, A.J.; Zhang, C.Y.; Omatsu, T.; Pask, H.M. An intracavity, frequency-doubled self-Raman vortex laser. *Opt. Express* **2014**, *22*, 5400–5409. [CrossRef]
31. Hu, W.W.; Li, Y.L.; Hu, C.W.; Gu, X.K.; Liu, H.X.; Zhang, Y.P.; Zhang, Y.M. Intra-cavity cascaded pumped 912nm/1030nm dual wavelength laser output. *Opt. Commun.* **2019**, *452*, 440–444. [CrossRef]
32. Liu, Y.; Dong, Y.; Xiao, H.D.; Yu, Y.J.; Jin, G.Y. Construction of 879 nm direct intra-cavity pumped dual-wavelength laser operating at 912 nm and 1064 nm. *Opt. Laser Technol.* **2019**, *115*, 477–480. [CrossRef]
33. Wang, S.; Zhao, Z.; Ito, I.; Kobayashi, Y. Direct generation of femtosecond vortex beam from a Yb:KYW oscillator featuring a defect-spot mirror. *OSA Continuum.* **2019**, *2*, 523–530. [CrossRef]
34. Liu, Y.; Dong, Y.; Yu, Y.J.; Wang, C.; Zhang, X.M. Output characteristics of no gain competition 912 nm and 1064 nm dual-wavelength lasers. *Opt. Laser Technol.* **2019**, *115*, 125–128. [CrossRef]